applied optics

Effect of sensor SNR and extinction ratio on polarimetric imaging error for nanowire-based systems

He Sun,[1,2] Dejiang Wang,[1,*] Cheng Chen,[1] Kehui Long,[1] and Xueqian Sun[2]

[1]Changchun Institute of Optics, Fine Mechanics and Physics, Chinese Academy of Sciences, Changchun 130033, China
[2]Graduate School of the Chinese Academy of Sciences, Beijing 100084, China
*Corresponding author: wangdj04@ciomp.ac.cn

Received 4 June 2018; revised 27 July 2018; accepted 27 July 2018; posted 27 July 2018 (Doc. ID 332998); published 29 August 2018

High-sensor SNR and high extinction ratio (ER), which are often contradictory requirements for nanowire-filter-based polarimetric imaging systems, aid in attenuating polarimetric imaging system errors. Expressions were derived to analyze their attenuation effects and then simplified using photoelectronic numbers received by superpixels (PNRS). The first-derivative ratios of PNRS and ER were calculated to compare their attenuation effects. Mathematical models and experiments conducted using polarimetric imaging systems with various ERs and PNRSs indicate that systems with low PNRS and high ER exhibit a polarization error affected more by the attenuation effect of the PNRS than that of the ER. When the system ER is higher than 28, the attenuation effect of the PNRS is higher than that of the ER. Thus, system error attenuation is a trade-off between sensor SNR and ER.

OCIS codes: (110.5405) Polarimetric imaging; (120.5410) Polarimetry; (230.5440) Polarization-selective devices; (260.5430) Polarization.

https://doi.org/10.1364/AO.57.007344

1. INTRODUCTION

Due to recent improvements in nanotechnology, polarimetric imaging systems with nanowire filters are now widely used in both commercial and military applications; they are lightweight and small, capable of tracking moving targets, and exhibit low susceptibility to temperature and vibrational effects [1–11]. Detector SNR and extinction ratio (ER) are the two main system parameters that greatly influence system errors; furthermore, it is known that system errors are low when the detector SNR is high or the ER is high. However, high detector SNR and high ER are contradictory requirements for nanowire-based polarimetric imaging systems. For example, high-full-well detectors are required to increase sensor SNR when shot noise is dominant in the imaging system; however, this means that detectors with a large pixel size must be employed, which results in a low ER [12,13]. In remote sensing, where a small focal number, F#, is employed for higher input light intensity in order to increase sensor SNR, the ER decreases because of cross talk [14,15]. Thus, it is not currently possible to determine the trade-off between these two parameters when trying to decrease system errors.

Nanowire-based polarimetric imaging system errors are usually divided into the categories of instantaneous field-of-view errors [8], which are caused by spatial resolution loss and are beyond the scope of this study, and polarization errors, which are comprised of nonuniformity errors and random errors. Bear Powell and Gruev [8] developed methods for correcting fixed-pattern nonuniformity errors to decrease the remaining nonuniformity errors. Perkins and Gruev analyzed the influence of different configurations of micropolarization filter arrays with the same optical performance (such as transmittance and ER) on random polarization errors, and they derived a four-polarizer nanowire-based system, on which the current study is based, in order to obtain lower random error [16]. Chen *et al.* analyzed the attenuation effect of the sensor SNR on system errors; however, their analysis indicated that there is no effect due to the ER [17]. To the best of our knowledge, there are no reports on the theoretical or experimental analysis of the attenuation effect of the sensor SNR and ER on nanowire-filter-based polarimetric imaging system errors.

Thus, in Section 2, we first derive mathematical models for detector noise (which reflect the sensor SNR directly), ER, and system polarization error and then use the photoelectronic numbers received by superpixels (PNRS) to determine the detector SNR in order to simplify our expressions. Then, the first-derivative ratio of the PNRS and the ER is calculated in order to compare their contributions to the polarization error.

In Section 3.A, an error measurement system that was developed for the polarimetric imaging system in order to quantitatively verify these models is presented. The F# of the lens was changed in order to create polarimetric imaging systems with variable ER (7, 20, 28, and 44). A polarimetric imaging system was constructed with an ER of 500 for comparison with the other imaging systems, and time division was employed for this system. We thus constructed five systems with different ERs. Seven different exposure times were used to modify the PNRS for each system with a different ER. In Section 3.B, the polarization random error and total polarization error after nonuniformity correction were calculated for these systems. A curve-fitting method was employed in order to derive the first-derivative ratio values of the PNRS and the ER for the experimental results, which were then compared with those of the mathematical models. Real-life images were also captured by systems with different ERs and PNRSs to further verify the results of the mathematical models.

2. ERRORS IN A NANOWIRE-FILTER-BASED SYSTEM

A. Mathematical Model of System Error

The linear polarimetric imaging system shown in Fig. 1 consists of a normal optical system and polarization sensor [14].

In order to compare the attenuation effects of the PNRS and the ER with respect to random polarization errors, a mathematical model of a nanowire-based polarimetric imaging system was derived. This system is a typical snapshot imaging system in which a random polarization error (σ_{random}) and a remaining nonuniformity error (σ_{nonuni}) are the two dominant error sources. Their relationship with the total polarization error (σ_{system}) can be described as $\sigma^2_{\text{total}} = \sigma^2_{\text{random}} + \sigma^2_{\text{nonuni}}$ [18]. The actual σ_{nonuni} is much lower than random noise after correction; in addition, there is currently no research to prove that the sensor SNR and ER will affect σ_{nonuni}. Thus, only the total error is analyzed in the experiments.

The image random noise is divided into the noise equivalent degree of linear polarization (NeDOLP, which is the variance of DOLP in the time domain) and the noise equivalent angle of linear polarization (NeAOLP, which is the variance of the angle of linear polarization, AOLP, in the time domain). NeDOLP and NeAOLP are derived as follows.

The photoelectronic numbers (PN) received by one pixel in the superpixel through a nanowire filter are described in Ref. [19], and they can be written as

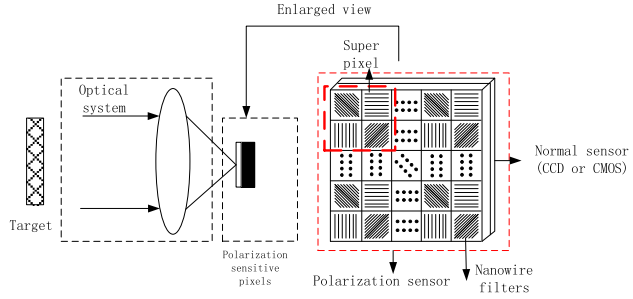

Fig. 1. DOLP (degree of linear polarization) imaging polarimeter system.

$$\mathrm{PN}^{\mathrm{out}}(\theta) = 0.5 \cdot \beta \cdot \mathrm{S0}_{\mathrm{in}} \cdot (\varepsilon^p + \varepsilon^q) \cdot \left\{1 + \frac{\varepsilon^p - \varepsilon^q}{\varepsilon^p + \varepsilon^q} \cdot \mathrm{DOLP}^{\mathrm{in}} \cdot \cos[2(\theta - \varphi)]\right\}, \quad (1)$$

where $\mathrm{PN}^{\mathrm{out}}(\theta)$ is the PN that is received by a photodetector (one pixel in a superpixel) after passing through a nanowire filter with orientation θ; ε^p is the transmittance of the pass axis; ε^q is the transmittance of the stop axis; and, these two parameters of the polarization sensor can be measured precisely [8]. $\mathrm{S0}_{\mathrm{in}}$ is the input target light intensity, $\mathrm{DOLP}^{\mathrm{in}}$ is the polarization degree of the input target light, φ is the polarization angle of the input target light, and β is the quantum efficiency of the photodetector.

In addition, the relationship between the PN received by the different pixels in one superpixel and the input target light polarization state (i.e., DOLP and AOLP) is given by

$$\mathrm{AOLP}^{\mathrm{in}} = 0.5 \cdot \frac{180}{\pi} \cdot a\tan\left\{\frac{[\mathrm{PN}^{\mathrm{out}}(0) - \mathrm{PN}^{\mathrm{out}}(90)]}{[\mathrm{PN}^{\mathrm{out}}(45) - \mathrm{PN}^{\mathrm{out}}(135)]}\right\}, \quad (2)$$

$$\mathrm{DOLP}^{\mathrm{in}} = \frac{2}{x} \cdot \frac{\sqrt{(\mathrm{PN}^{\mathrm{out}}(0) - \mathrm{PN}^{\mathrm{out}}(90))^2 + (\mathrm{PN}^{\mathrm{out}}(45) - \mathrm{PN}^{\mathrm{out}}(135))^2}}{(\mathrm{PN}^{\mathrm{out}}(0) + \mathrm{PN}^{\mathrm{out}}(90) + \mathrm{PN}^{\mathrm{out}}(45) + \mathrm{PN}^{\mathrm{out}}(135))}, \quad (3)$$

where $\mathrm{PN}^{\mathrm{out}}$ (0), $\mathrm{PN}^{\mathrm{out}}$ (90), $\mathrm{PN}^{\mathrm{out}}$ (45), and $\mathrm{PN}^{\mathrm{out}}$ (135) are the PNs received by the pixels with the corresponding angle in one superpixel, and x is the diattenuation of one nanowire filter in the superpixel. The latter can be calculated using the expression $x = (\varepsilon^p - \varepsilon^q)/(\varepsilon^p + \varepsilon^q)$, as there is no significant difference between the diattenuation of the four pixels in one superpixel [8]. The relationship between the diattenuation and the ER can be described as $x = (\mathrm{ER} - 1)/(\mathrm{ER} + 1)$.

The diattenuation of a superpixel can be measured precisely [14]. Thus, the main error in $\mathrm{AOLP}^{\mathrm{in}}$ and $\mathrm{DOLP}^{\mathrm{in}}$ in Eqs. (2) and (3) is due to the random PN error from the sensor. For a scientific imaging sensor, the random error is composed of shot, dark, and read noise. Now, the total of the dark and read noise in a scientific sensor is usually less than 0.05% of the full-well capacity [20]. In this case, when the PN received by the imaging sensor is greater than 2% of the full-well capacity, we only need to consider the shot noise. Thus, the variance of the received photons is caused by the shot noise alone and follows a Poisson distribution, $\sigma_{\text{shot}} = \sqrt{\mathrm{PN}}$ [16]; and, at this time, sensor SNR is $\mathrm{SNR}_{\text{sensor}} = \text{signal}/\sigma_{\text{shot}} = \sqrt{\mathrm{PN}}$.

We use error propagation methods to determine the uncertainty in the AOLP and DOLP. If we consider the error propagation of the AOLP as an example, we have [21,22]

$$\mathrm{NeDOLP}^{\mathrm{in}} = \left(\frac{\partial \mathrm{DOLP}_{\mathrm{in}}}{\partial \mathrm{PN}^{\mathrm{out}}(0)}\right)^2 \cdot \sigma^2_{\mathrm{PN}^{\mathrm{out}}(0)} + \left(\frac{\partial \mathrm{DOLP}_{\mathrm{in}}}{\partial \mathrm{PN}^{\mathrm{out}}(90)}\right)^2 \cdot \sigma^2_{\mathrm{PN}^{\mathrm{out}}(90)} + \left(\frac{\partial \mathrm{DOLP}_{\mathrm{in}}}{\partial \mathrm{PN}^{\mathrm{out}}(45)}\right)^2 \cdot \sigma^2_{\mathrm{PN}^{\mathrm{out}}(45)} + \left(\frac{\partial \mathrm{DOLP}_{\mathrm{in}}}{\partial \mathrm{PN}^{\mathrm{out}}(135)}\right)^2 \cdot \sigma^2_{\mathrm{PN}^{\mathrm{out}}(135)}. \quad (4)$$

Solving $\mathrm{NeDOLP^{in}}$ from Eq. (2), we have

$$\mathrm{NeDOLP^{in}} = \frac{2 * (\mathrm{ER} + 1)}{[\mathrm{DOLP^{in}} \cdot (\beta \cdot \mathrm{S0_{in}} \cdot (\varepsilon^p + \varepsilon^q))^{\frac{1}{2}} \cdot (\mathrm{ER} - 1)]}, \tag{5}$$

where $\mathrm{S0_{in}}$, β, and $(\varepsilon^p + \varepsilon^q)$ are dependent on the system status; however, these do not directly represent the working status of the current system. Thus, we use the variate PNRS described in Eq. (6), which represents the PN currently received by the superpixel and is the direct representation of the current imaging system; this can be easily determined when the system is working:

$$\begin{aligned}\mathrm{PNRS} = 0.5 \cdot (&\mathrm{PN^{out}}(0) + \mathrm{PN^{out}}(90) \\ &+ \mathrm{PN^{out}}(45) + \mathrm{PN^{out}}(135)).\end{aligned} \tag{6}$$

By combining Eqs. (1)–(6), we obtain

$$\mathrm{PNRS} = \beta \cdot \mathrm{S0_{in}} \cdot (\varepsilon^p + \varepsilon^q). \tag{7}$$

Thus,

$$\mathrm{NeDOLP^{in}} = 2 \cdot \left[\frac{1}{(\mathrm{PNRS})^{\frac{1}{2}}}\right] \cdot \left(1 + \frac{2}{\mathrm{ER} - 1}\right). \tag{8}$$

Similarly,

$$\mathrm{NeAOLP^{in}} = \frac{14.35}{[\mathrm{DOLP^{in}}]} \times \mathrm{NeDOLP^{in}}. \tag{9}$$

The difference in the $\mathrm{NeDOLP^{in}}$ and the $\mathrm{NeAOLP^{in}}$ is the coefficient $14.35/\mathrm{DOLP^{in}}$, which means the attenuation effect comparison of the ER and PNRS on the DOLP and AOLP errors is the same. Therefore, it is necessary only to analyze the $\mathrm{NeDOL}P^{\mathrm{in}}$ in order to obtain a result that will also fit $\mathrm{NeAOLP^{in}}$.

B. Analysis of Mathematical Model

In order to compare the attenuation of the ER and the PNRS, which are two different physical quantities with different dimensions, we use their maximum value in engineering and introduce the relative variates PNRSB and ERB to normalize the PNRS and the ER. When the range of the ER is $[\mathrm{ER_{min}}, \mathrm{ER_{max}}]$ and the range of PNRS is $[\mathrm{PNRS_{min}}, \mathrm{PNRS_{max}}]$, the PNRS in Eq. (8) becomes $\mathrm{PNRSB} \cdot \mathrm{PNRS_{max}}$, and the ER in Eq. (8) becomes $\mathrm{ERB} \cdot \mathrm{ER_{max}} + 1$. The PNRSB and ERB indicate the percentage by which these two parameters can increase. For example, a PNRSB of nearly 0.9 indicates that the PNRS of the current system is almost at the maximum value and can only increase a little. Thus, we may derive the following expression:

$$\mathrm{NeDOLP} = \frac{200}{(\mathrm{PNRSB} \cdot \mathrm{PNRS_{max}})^{\frac{1}{2}}} \cdot \left[1 + \frac{2}{\mathrm{ERB} * \mathrm{ER_{max}}}\right]. \tag{10}$$

We can deduce the first derivatives of the PNRS ($\mathrm{diff}_{\mathrm{PNRSB}}^{\mathrm{NeDOLP}}$) and the ER ($\mathrm{diff}_{\mathrm{ERB}}^{\mathrm{NeDOLP}}$), which quantitatively reflect their attenuation effects on the NeDOLP; their ratio may then be obtained in order to compare their attenuation effects. The ratio is $\mathrm{COM_{diff}} = \mathrm{diff}_{\mathrm{PNRSB}}^{\mathrm{NeDOLP}} / \mathrm{diff}_{\mathrm{ERB}}^{\mathrm{NeDOLP}}$, which can be derived as

$$\mathrm{COM_{diff}} = \frac{\mathrm{ERB} \cdot (\mathrm{ERB} \cdot \mathrm{ER_{max}} + 2)}{4 \cdot \mathrm{PNRSB}}. \tag{11}$$

We can see from Eq. (11) that a lower PNRSB and a higher ERB contribute to increase the $\mathrm{COM_{diff}}$. Thus, we arrive at our first conclusion: if the current system has a relatively high ER and low PNRS, which is caused by an inappropriate exposure strategy, a high F#, or a small full-well capacity, the first priority when aiming to lower system noise is to increase the PNRS rather than to increase the ER.

Since MAX(PNRSB) = 1, we can deduce that

$$\mathrm{COM_{diff}} < \frac{\mathrm{ERB} \cdot (\mathrm{ERB} \cdot \mathrm{ER_{max}} + 2)}{4}. \tag{12}$$

Owing to the limitations of nanotechnology, the maximum ER for the current polarimetric imaging system based on a nanowire filter is 100 [19,23]; and, we know from Eq. (12) that when ER is higher than 20, $\mathrm{diff}_{\mathrm{PNRSB}}^{\mathrm{NeDOLP}}$ is higher than $\mathrm{diff}_{\mathrm{ERB}}^{\mathrm{NeDOLP}}$. This means that the attenuation effect on the system polarization error due to an increase in the PNRS is always higher than that caused by an increase in the ER, which is the second conclusion. Further, we know that when better nanotechnology methods are employed, the maximum ER of a polarimetric imaging system based on a nanowire filter can reach 200. Where the ER is more than 28, $\mathrm{diff}_{\mathrm{PNRSB}}^{\mathrm{NeDOLP}}$ is higher than $\mathrm{diff}_{\mathrm{ERB}}^{\mathrm{NeDOLP}}$. Furthermore, when the ER and the PNRS increase by the same multiples, which means that when the ER increases from ER1 to $N * \mathrm{ER1}$, PNRS increases from PNRS1 to $N * \mathrm{PNRS1}$, we can have one $\mathrm{PNRS_{max}}$ to get

$$\begin{cases} \mathrm{ERB1} = \frac{\mathrm{ER1}}{\mathrm{ER_{max}}} = \mathrm{PNRSB1} = \frac{\mathrm{PNRS1}}{\mathrm{PNRS_{max}}} \\ \mathrm{ERB2} = \frac{\mathrm{N \cdot ER1}}{\mathrm{ER_{max}}} = \mathrm{PNRSB2} = \frac{\mathrm{N \cdot PNRS1}}{\mathrm{PNRS_{max}}} \end{cases}. \tag{13}$$

At this time, when the ER is higher than 40, $\mathrm{COM_{diff}}$ is greater than 10, which implies that when PNRS and ER increase by the same multiples, the attenuation due to the PNRS is 10 times higher than that due to the ER, irrespective of the value of $\mathrm{ER_{max}}$. This is our third conclusion. Among them, the first and second conclusions are verified by experiments in the next section.

The mathematical model presented above is not restricted to a polarimetric system based on a nanowire filter. As long as the system is constructed using four analyzer angles, as mentioned above, this model may be employed. This study focuses on a polarimetric system based on a nanowire filter, as its maximum extinction is relatively low, which led to some of the characteristics of this model; and in this system, a higher PNRS is often incompatible with a higher ER.

3. EXPERIMENTS AND RESULTS

A. Experimental Setup

In order to validate the mathematical model, we constructed a polarization error measurement system to measure the random polarization errors and total polarization errors of polarimetric imaging systems with variable ERs and PNRSs. The error measurement system is shown in Fig. 2, and it is comprised of an integrated sphere (A), a collimator (B), a wide-cutoff visible

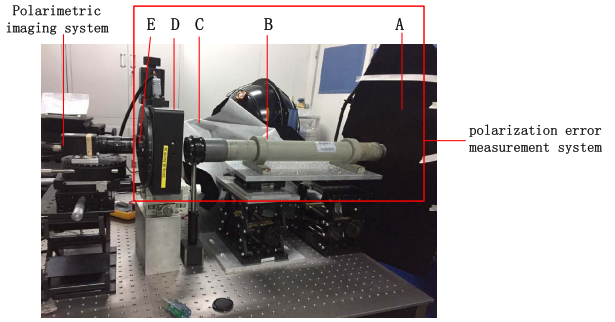

Fig. 2. Experimental apparatus.

Table 1. Different ERs for Different F Numbers

F#	2	4	22
ER	20	28	44

bandpass filter (C), and a precision hollow rotary table (D) containing a polarizer (E, analyzer). The polarization state of the light output from the analyzer could be changed accurately in the visible band [8]. Compared to other methods for creating controllable polarized light, such as liquid crystal modulation [24] or parallel glass plates [3,21], the advantage of the selected method is that it provides a broadband spectrum and a large divergence angle, both of which are useful in engineering applications.

To construct polarimetric imaging systems with ERs of 20, 28, and 44, we used a method in which the F# of the lens was adjusted [14]. The corresponding parameters are listed in Table 1. All of these systems employed a polarimetric imaging camera from 4D Technology [25,26].

Systems with ER values of 7 [14] are shown in Fig. 3(a). Since the mathematical model is also suited for systems with a normal polarizer, we constructed the system shown in Fig. 3(b). The ER of this system is 500.

B. Experiments of System Polarization Error

The nonuniformity of polarimetric imaging systems must be corrected [8]. We use the method outlined in Ref. [8] for each system with a different ER value.

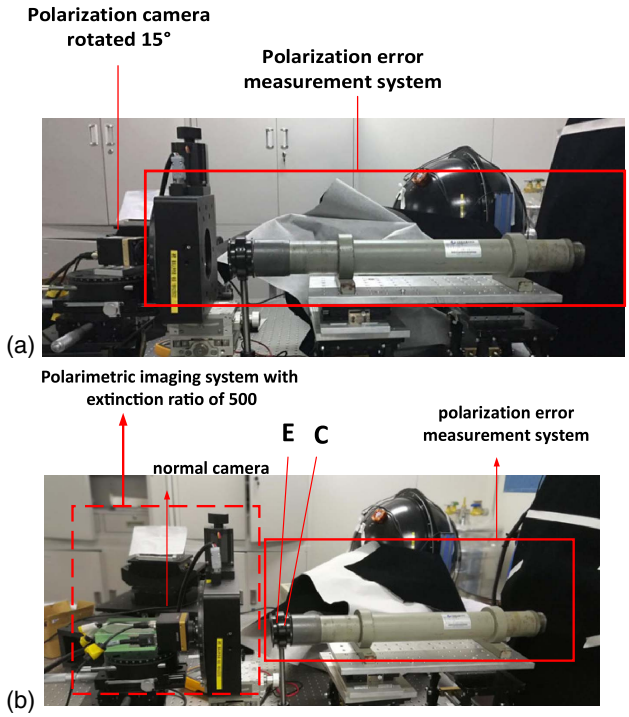

Fig. 3. Experimental apparatus for (a) ER = 7 and (b) ER = 500.

During the experiment, we have five different ER values, named ER_sn, as shown in Eq. (14):

$$\text{ER\_sn} = [7, 20, 28, 44, 500]. \tag{14}$$

The PNRS in the experiment varied from 7–26 Ke^-. As the PNRS varied in one sensor, the average PN received by the superpixel was used in the experiment. The average PN values are given by PNRS_sn, as shown in Eq. (15):

$$\text{PNRS\_sn} = [7.4\text{K}, 9.9\text{K}, 12.6\text{K}, 15.7\text{K}, 21.3\text{K}, 24\text{K}, 27\text{K}], \quad (\text{K} = 10^3 e^-). \tag{15}$$

Thus, 35 (5 × 7) experiments were conducted, and each experiment contained 32 different sets of data for the analyzer angles, which were averaged to obtain the final results [18]. The final picture data set is $\text{pic}_{i,j,\theta,n}$. The rows and columns are represented by i and j; θ is the analyzer angle; and n represents the index of pictures captured during each analyzer angle. The experimental random polarization error can be calculated using Eqs. (16) and (17):

$$\text{NeAOLP}^{\text{exp}}_{\text{random}} = \sqrt{\left(\sum_{\theta}\left(\sum_{n-1}\left(\sum_{i,j}(\text{AOLP\_pic}_{i,j,\theta,n} - \text{AOLP\_pic}_{i,j,\theta,n+1})^2\right)/(2\cdot(i\cdot j))\right)/(n-1)\right)/32}, \tag{16}$$

$$\text{NeDOLP}^{\text{exp}}_{\text{random}} = \sqrt{\left(\sum_{\theta}\left(\sum_{n-1}\left(\sum_{i,j}(\text{DOLP\_pic}_{i,j,\theta,n} - \text{DOLP\_pic}_{i,j,\theta,n+1})^2\right)/(2\cdot(i\cdot j))\right)/(n-1)\right)/32}. \tag{17}$$

Experimental random polarization error can be caused by various types of system noise, and the actual PNRS calculated for a digital system is not entirely realistic. These two factors lead to deviations between the simulation data and the experimental data. However, we only focus on a comparison of the PNRS and ER attenuation effects on polarization error. As a

result, we use the normalized method in order to address the experimental and simulation data. Both the experimental and simulation random errors [calculated using Eqs. (8) and (9)] are divided by their average values. There are, in total, 35 experimental DOLP errors and simulation DOLP errors, and their average values are 1.28 and 1.09, respectively. Thus, the experimental and simulation random DOLP errors are divided by 1.28 and 1.09, respectively. Using the same method to deal with AOLP errors, the experimental and simulation random AOLP errors are divided by 0.41 and 0.32, respectively. The results are shown in Fig. 4, where dashed lines show the normalized simulation results for different ER systems calculated from Eqs. (8) and (9). Solid lines with triangles represent the normalized experimental results for the different ER systems.

The total polarization noise is calculated as

$$\mathrm{NeAOLP}_{\mathrm{noise}} = \partial(\mathrm{AOLP\_pic}_{\theta,n}), \tag{18}$$

$$\mathrm{NeDOLP}_{\mathrm{noise}} = \partial(\mathrm{DOLP\_pic}_{\theta,n}). \tag{19}$$

The normalized experimental total noise and simulation random noise are shown in Fig. 5. They have been divided by their average values, using the same method as for the random errors.

A data-fitting method was employed to derive $\mathrm{COM}_{\mathrm{diff}}$ from the experimental results. The experimental data-fitting procedure is as follows:

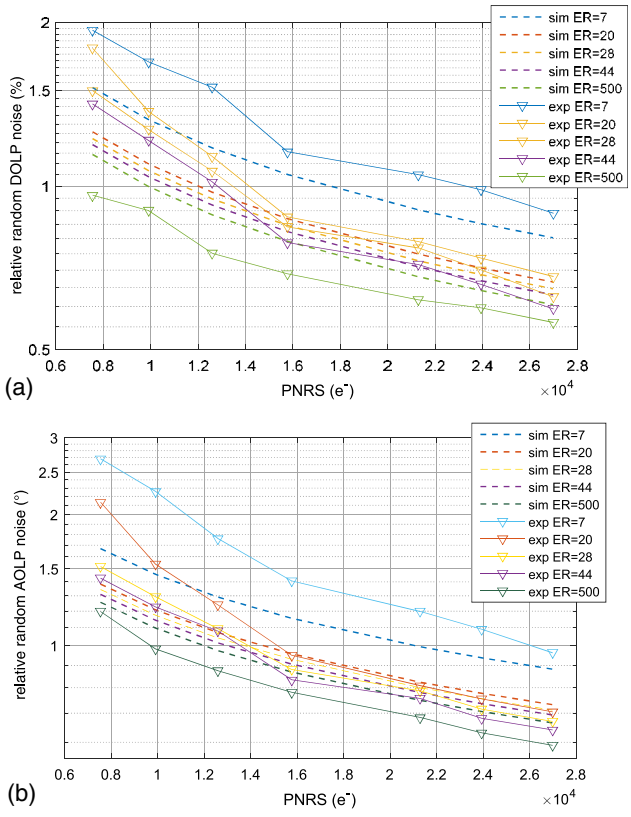

Fig. 4. Experimental and simulation random polarization noise for (a) DOLP and (b) AOLP.

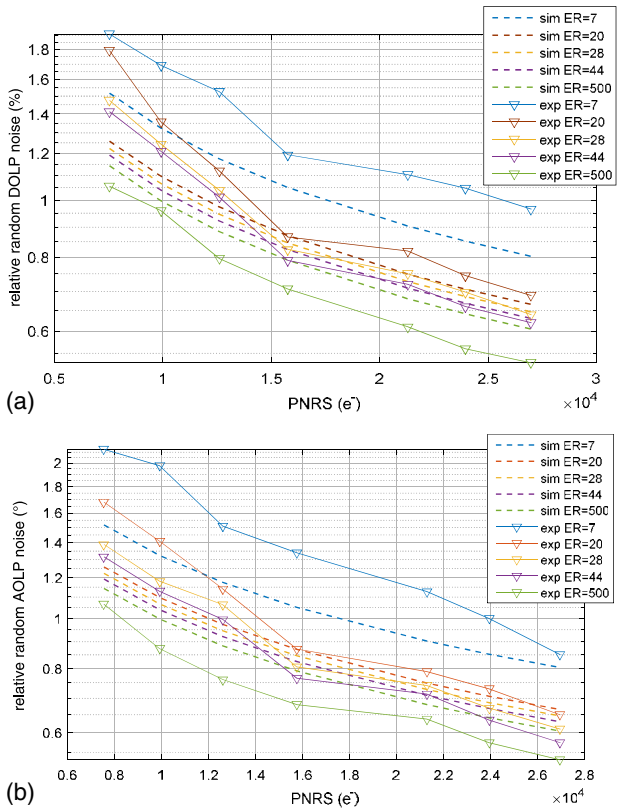

Fig. 5. Normalized experimental total noise and simulation random polarization noise for (a) DOLP and (b) AOLP.

1. Curve fitting. Consider the process to derive a functional relationship between the ER and the NeDOLP, as an example. ER, and the corresponding NeDOLP, are split into seven groups, according to the PNRS value. In each group, we fit curves between ER and NeDOLP that have the form $f(x) = ax^b + c$. We rewrite ER as $\mathrm{ERB} \cdot \mathrm{ER}_{\mathrm{max}} + 1$ and, finally, derive the normalized function $\mathrm{fN}_{\mathrm{ER}}(\mathrm{ERB})$ ($N = 1$–7). Similarly, $\mathrm{fN}_{\mathrm{PNRS}}$ (PNRSB) ($N = 1$–7, N for different ER groups) can also be derived.
2. We deduce the first-derivative functions for the ER and the PNRS, $\mathrm{diff}_{\mathrm{fN}_{\mathrm{ER}}(\mathrm{ERB})}$ and $\mathrm{diff}_{\mathrm{fN}_{\mathrm{PNRS}}(\mathrm{PNRSB})}$, respectively.
3. Then, we take the normalized ERB, given by $\mathrm{ER}_{\mathrm{sn}}/\mathrm{ER}_{\mathrm{max}}$, and the PNRSB value, given by $\mathrm{PNRS}_{\mathrm{sn}}/\mathrm{PNRS}_{\mathrm{max}}$, and use the first-derivative function to derive the $\mathrm{COM}_{\mathrm{diff}}$ value. The lower the $\mathrm{PNRS}_{\mathrm{max}}$ value is, then the lower the $\mathrm{diff}_{\mathrm{fN}_{\mathrm{PNRS}}(\mathrm{PNRSB})}$ will be. We choose $\mathrm{PNRS}_{\mathrm{max}}$ to be 27 Ke^- and $\mathrm{ER}_{\mathrm{max}}$ to be 100, in order to have a relatively low $\mathrm{diff}_{\mathrm{fN}_{\mathrm{PNRS}}(\mathrm{PNRSB})}$. In fact, 27 Ke^- is the maximum PNRS in our experiment, but it would be higher if a higher-well-capacity sensor or better auto exposure strategy were employed. An ER of 100 is currently the largest-extinction-ratio polarimetric imaging system based on a nanowire filter.
4. Finally, we calculate the $\mathrm{COM}_{\mathrm{diff}}$ value of the NeDOLP and NeAOLP.

The comparison figures for the simulation and experiments with the same $\mathrm{PNRS}_{\mathrm{max}}$ and $\mathrm{ER}_{\mathrm{max}}$ are shown in Figs. 6 and 7. The solid line denotes the experimental result based on the data process mentioned above. The dashed line is

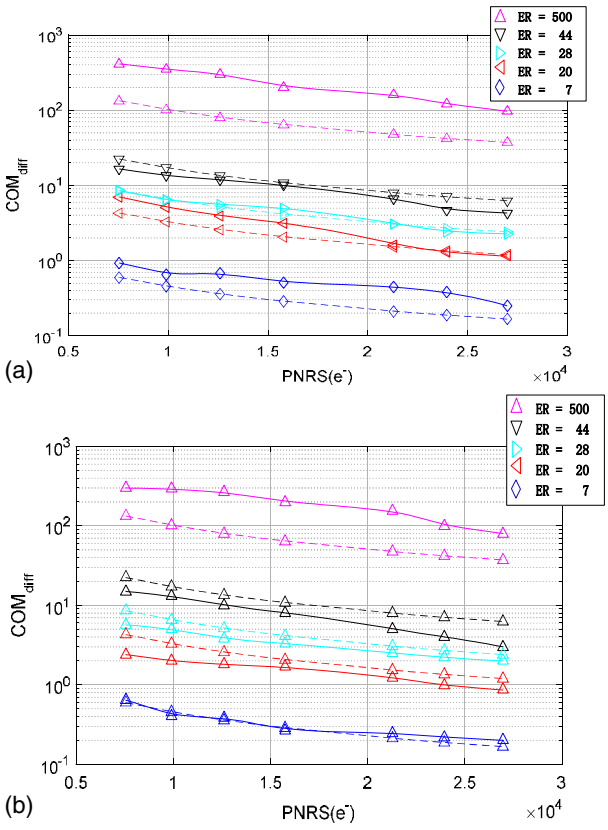

Fig. 6. Experimental results for COM_{diff} values with random (a) NeDOLP and (b) NeAOLP.

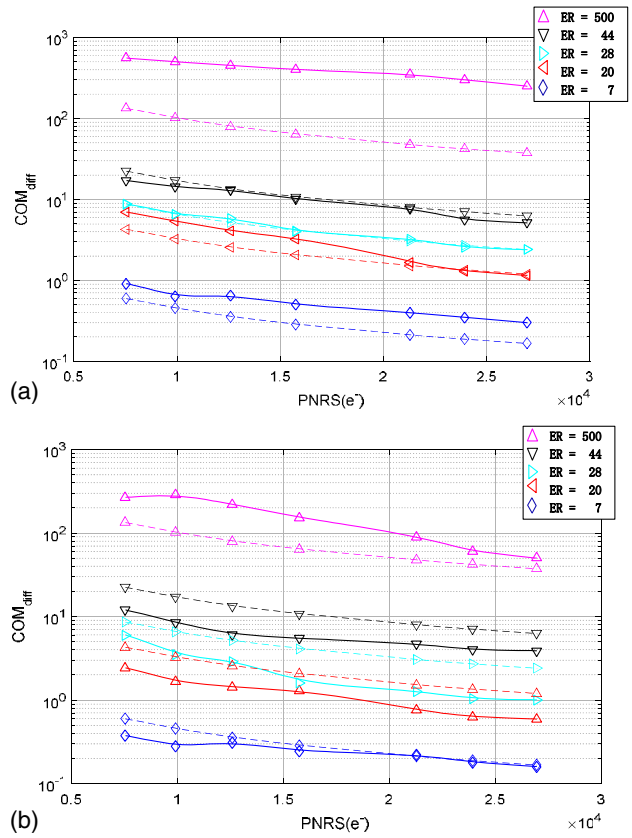

Fig. 7. Experimental results for COM_{diff} values with total (a) NeDOLP and (b) NeAOLP.

the simulation result that corresponds to the actual ERB and PNRSB.

There are four key differences between the simulation and experimental data:

1. The difference between ER = 7 and ER = 20 in the experimental data is larger than that in the simulation. This may be caused by the cross talk effect when ER = 7. The performance of each nanowire filter cannot be regarded as a normal polarizer with the standard Mueller matrix.
2. Theoretically, when the ER is more than 20, COM_{diff} will be greater than 1. In the experiment, however, when the ER is more than 20 and PNRS is higher than 18,000, the COM_{diff} of the NeAOLP would be less than 1, which is caused by system cross talk and experimental error. This means that in cases where the PNRS can increase only by less than 34%, improving the ER could be a better choice for reducing error.
3. The difference between ER = 44 and ER = 500 in the experimental data is larger than that in the simulation data. This difference may result from difficulties in measuring a high ER accurately for such a wide spectral range.
4. When the PNRS is small, its influence in the experiment is larger than in the simulation. This is because the amount of sensor additive noise, such as detector dark current noise and quantization noise, is larger in the experiment. The mathematical model in this study only considers sensor noise to be shot noise.

Though errors exist in the experiments, we can also determine that the attenuation effects of the ER and the PNRS on the polarization degree and polarization angle are almost the same in the simulation and in the experiment. The curvilinear trends of the simulation and the experiments in Figs. 6 and 7 prove the first conclusion in Section 2.B: A lower PNRS and a higher ER lead to a higher COM_{diff} (the ratio of the attenuation effects of the PNRS and the ER), which implies that when the system based on a nanowire filter has a relatively high ER and low PNRS, using a higher-well-capacity sensor or better exposure strategy will have a greater attenuation effect than improving the system ER. We know that the attenuation effect of the PNRS will be higher than that of the ER when the ER is higher than 28, as per our experimental results, which is also our second conclusion in Section 2.B. This means that, currently, when the ER of a system based on a nanowire filter is higher than 28 (or the ER is higher than 20, and the PNRS is lower than 18 Ke^-), improving the PNRS instead of the ER must be the priority in order to attenuate the system error.

4. IMAGE ANALYSIS

In this section, we present images obtained from polarimetric imaging systems based on a nanowire filter to prove that under certain circumstances, improving the system PNRS has a better attenuation effect than improving the ER. The target in this

section is a Logitech M545 mouse covered in a large number of tiny dust particles. These dust particles could easily be seen by polarization images rather than intensity images. In the experiments, we use two systems with different ERs to image the target. One system has $F\# = 22$ (referred to as F22) and ER = 44, and the other system has $F\# = 2$ (referred to as F2) and ER = 20. In the experiments, the exposure time is adjusted to make the PNRS of F2 twice that of the PNRS of F22. Then, we choose two typical small parts, labeled A and B for the analysis, as shown in Fig. 8.

To quantitatively evaluate the pictures, we averaged 100 images as ideal images without noise. Other images based on a single shot were used to evaluate the images containing noise. The polarization imaging noise can be calculated as

$$\mathrm{NeDOLP}_{\mathrm{pic}} = \frac{\sqrt{\sum (\mathrm{DOLP}_{\mathrm{single}} - \mathrm{DOLP}_{\mathrm{aver}})^2}}{\mathrm{pix}_{\mathrm{num}}}, \tag{20}$$

$$\mathrm{NeAOLP}_{\mathrm{pic}} = \frac{\sqrt{\sum (\mathrm{AOLP}_{\mathrm{single}} - \mathrm{AOLP}_{\mathrm{aver}})^2}}{\mathrm{pix}_{\mathrm{num}}}. \tag{21}$$

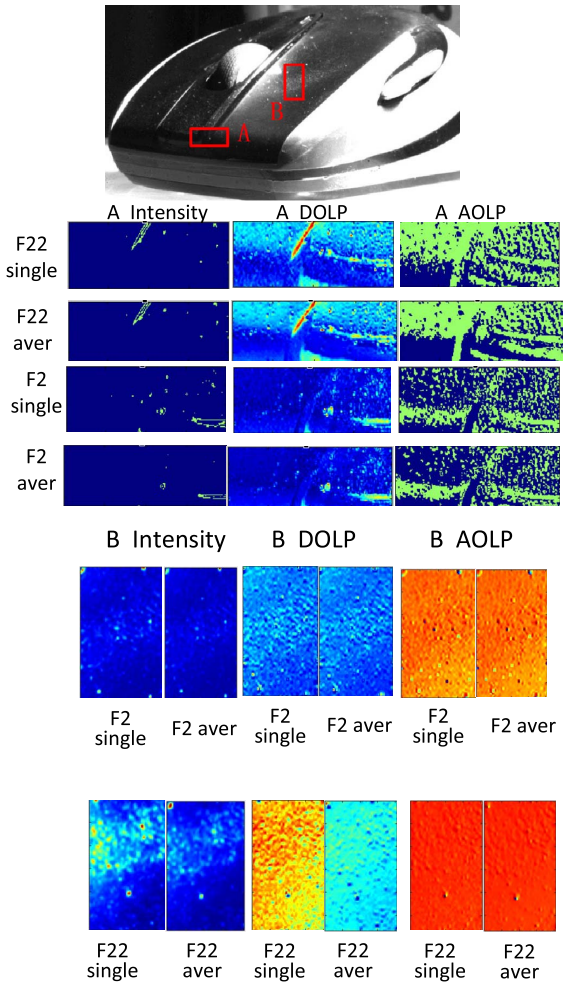

Fig. 8. Images obtained for a system with ER = 44 (F22) and ER = 20 (F2).

Table 2. Detailed Results for Areas A and B

Designated Area	System ER	PNRS (ke-)	DOLP (%)	NeDOLP (%)	NeAOLP (°)
A	44	4	55	3.76	5.1
A	20	10	55	3.15	3.98
B	44	0.45	33	8.78	10.4
B	20	1	33	4.87	6.79

A comparison of the results for areas A and B and for the F22 system (ER = 44) are listed in Table 2.

From these comparisons, it is apparent that in areas A and B, when the ER is lower and the PNRS is higher, the NeDOLP and NeAOLP are lower. When the initial PNRS is relatively high, at 4 Ke^-, the polarization accuracy is relatively low, at 16.2%. When the initial PNRS is relatively low, at 0.45×10^3, the polarization accuracy lower value is relatively high, at 44.8%. These results indicate that the attenuation effect of the PNRS on polarization accuracy is greater than that of the ER. This greater value is higher when the PNRSB is relatively low.

5. CONCLUSION

In this study, we analyzed the attenuation effects of the ER and the PNRS (which directly reflect sensor SNR) on system polarization error, theoretically and experimentally. First, our results indicate that for systems with a relatively higher ER and lower PNRS, $\mathrm{COM}_{\mathrm{diff}}$ will be higher, which means that the attenuation effect of the PNRS is more obvious. This conclusion fits well with the experimental results. Second, because the ER of the nanowire-based system is lower than 100, the attenuation effect of the PNRS will be always greater than that of the ER when the ER is higher than 20. In the experiments, however, this boundary value of 20 is increased to 28, owing to experimental errors and system cross talk. Real-life images were taken under particular conditions in order to prove that when the ER is higher and the PNRS is lower, the polarization error can increase by more than 17%. These findings indicate that in many circumstances, the PNRS plays a more important role in decreasing system error than the ER. However, systems based on nanowire filters contain multiple sources of errors, and the weights of these sources vary according to the different system constructions and imaging conditions. For instance, when the target spectral information differs considerably from the light source used in the nonuniformity correction, the nonuniformity error may be larger than the random error. In such a case, the directions provided in this study would require adjustment, and the issues related to such systems should be the subject of future investigations.

Funding. National Natural Science Foundation of China (NSFC) (61675202).

REFERENCES

1. Y. Liu, T. York, W. Akers, G. Sudlow, V. Gruev, and S. Achilefu, "Complementary fluorescence-polarization microscopy using division-of-focal-plane polarization imaging sensor," J. Biomed. Opt. **17**, 116001 (2012).

2. J. S. Tyo, D. L. Goldstein, D. B. Chenault, and J. A. Shaw, "Review of passive imaging polarimetry for remote sensing applications," Appl. Opt. **45**, 5453–5469 (2006).
3. J. L. Deuzé, F. M. Bréon, C. Devaux, P. Goloub, M. Herman, B. Lafrance, F. Maignan, A. Marchand, F. Nadal, G. Perry, and D. Tanré, "Remote sensing of aerosols over land surfaces from POLDER-ADEOS-1 polarized measurements," J. Geophys. Res. **106**, 4913–4926 (2001).
4. M. Zhang, X. Wu, N. Cui, N. Engheta, and J. Van der Spiegel, "Bioinspired focal-plane polarization image sensor design: from application to implementation," Proc. IEEE **102**, 1435–1449 (2014).
5. X. Zhao, F. Boussaid, A. Bermak, and V. G. Chigrinov, "High-resolution thin "guest-host" micropolarizer arrays for visible imaging polarimetry," Opt. Express **19**, 5565–5573 (2011).
6. K. Sasagawa, S. Shishido, K. Ando, H. Matsuoka, T. Noda, T. Tokuda, K. Kakiuchi, and J. Ohta, "Image sensor pixel with on-chip high extinction ratio polarizer based on 65-nm standard CMOS technology," Opt. Express **21**, 11132–11140 (2013).
7. M. Sarkar, D. S. S. Bello, C. van Hoof, and A. J. Theuwissen, "Biologically inspired CMOS image sensor for fast motion and polarization detection," IEEE Sens. J. **13**, 1065–1073 (2013).
8. S. Bear Powell and V. Gruev, "Calibration methods for division-of-focal-plane polarimeters," Opt. Express **21**, 21039–21055 (2013).
9. H. Park and K. B. Crozier, "Elliptical silicon nanowire photodetectors for polarization-resolved imaging," Opt. Express **23**, 7209–7216 (2015).
10. M. Garcia, C. Edmiston, R. Marinov, A. Vail, and V. Gruev, "Bio-inspired color-polarization imager for real-time in situ imaging," Optica **4**, 1263–1271 (2017).
11. Y. Maruyama, T. Terada, T. Yamazaki, Y. Uesaka, M. Nakamura, Y. Matoba, K. Komori, Y. Ohba, S. Arakawa, and Y. Hirasawa, "3.2-MP back-illuminated polarization image sensor with four-directional air-gap wire grid and 2.5-μm pixels," IEEE Trans. Electron Devices **65**, 2544–2551 (2018).
12. A. A. Cruz-Cabrera, S. A. Kemme, J. R. Wendt, R. R. Boye, T. R. Carter, and S. Samora, "Polarimetric imaging cross talk effects from glue separation between FPA and micropolarizer arrays at the MWIR," Proc. SPIE **6478**, 64780Q (2007).
13. D. A. Miller, D. W. Wilson, and E. L. Dereniak, "Novel design and alignment of wire-grid diffraction gratings on a visible focal plane array," Opt. Eng. **51**, 014001 (2012).
14. V. Gruev, R. Perkins, and T. York, "CCD polarization imaging sensor with aluminum nanowire optical filters," Opt. Express **18**, 19087–19094 (2010).
15. G. P. Nordin, J. T. Meier, P. C. Deguzman, and M. W. Jones, "Diffractive optical element for Stokes vector measurement with a focal plane array," Proc. SPIE **3754**, 169–177 (1999).
16. R. Perkins and V. Gruev, "Signal-to-noise analysis of Stokes parameters in division of focal plane polarimeters," Opt. Express **18**, 25815–25824 (2010).
17. Z. Chen, X. Wang, S. Pacheco, and R. Liang, "Impact of CCD camera SNR on polarimetric accuracy," Appl. Opt. **53**, 7649–7656 (2014).
18. J. D. Agosino and C. Webb, "3-D analysis framework and measurement methodology for imaging system noise," Proc. SPIE **1488**, 194–203 (1991).
19. J. S. Tyo, C. F. LaCasse, and B. M. Ratliff, "Total elimination of sampling errors in polarization imagery obtained with integrated microgrid polarimeters," Opt. Lett. **34**, 3187–3189 (2009).
20. "GSENSE400_Datasheet_V1.2.0," GPIXEL Inc., 2013.
21. K. Qing, L. Jianjun, C. Ligang, W. Haoyu, Y. Yinlin, M. Fangang, Z. Wenchao, Q. Tao, and Z. Xiaobing, "Test and uncertainty analysis of reference source with variable polarization degree and large dynamic range," Acta Opt. Sin. **35**, 0412003 (2015).
22. P. R. Bevington and D. K. Robinson, *Data Reduction and Error Analysis for the Physical Sciences* (McGraw-Hill, 1992), pp. 42–43.
23. J. J. Wang, F. Walters, X. Liu, P. Sciortino, and X. Deng, "High-performance, large area, deep ultraviolet to infrared polarizers based on 40 nm line/78 nm space nanowire grids," Appl. Phys. Lett. **90**, 061104 (2007).
24. X. Zhao, A. Bermak, F. Boussaid, and V. G. Chigrinov, "Liquid-crystal micropolarimeter array for full Stokes polarization imaging in visible spectrum," Opt. Express **18**, 17776–17787 (2010).
25. "KAI-2020 image sensor device performance specification," Eastman Kodak Company, 2010.
26. "4D's polarimetric imaging camera based on nano-wire filter [EB/OL]," https://www.4dtechnology.com/products/polarimeters/polarcam/.